A high-temperature anion-exchange membrane fuel cell with a critical raw material-free cathode

Douglin, J.C.; Singh, R.K.; Haj-Bsoul, S.; Li, S.; Biemolt, J.; Yan, N.; Varcoe, J.R.; Rothenberg, G.; Dekel, D.R.

DOI
10.1016/j.ceja.2021.100153

Publication date
2021

Document Version
Final published version

Published in
Chemical Engineering Journal Advances

Chemical Engineering Journal Advances 8 (2021) 100153

Contents lists available at ScienceDirect

Chemical Engineering Journal Advances

journal homepage: www.sciencedirect.com/journal/chemical-engineering-journal-advances

A high-temperature anion-exchange membrane fuel cell with a critical raw material-free cathode

John C. Douglin [a], Ramesh K. Singh [a,b], Saja Haj-Bsoul [a], Songlin Li [a], Jasper Biemolt [c], Ning Yan [c], John R. Varcoe [d], Gadi Rothenberg [c], Dario R. Dekel [a,b,*]

[a] The Wolfson Department of Chemical Engineering, Technion – Israel Institute of Technology, Haifa 3200003, Israel
[b] The Nancy & Stephen Grand Technion Energy Program (GTEP), Technion – Israel Institute of Technology, Haifa 3200003, Israel
[c] Van 't Hoff Institute for Molecular Sciences University of Amsterdam, Science Park 904 1098 XH Amsterdam, the Netherlands
[d] Department of Chemistry, University of Surrey, Guildford GU2 7XH, United Kingdom

ARTICLE INFO

Keywords:
Anion-exchange membrane fuel cells
HT-AEMFC
Critical raw materials-free
PGM-free
oxygen reduction reaction
N-doped-C

ABSTRACT

We present a first high-temperature anion-exchange membrane fuel cell (HT-AEMFC, operating at 105 °C) based on a critical raw material (CRM)-free cathode catalyst; at the same temperature, the anion-exchange membrane (AEM) has a high ex-situ hydroxide conductivity value of 201 mS cm^{-1}. Our HT-AEMFC, containing a highly active nitrogen-doped carbon (N-doped-C) cathode catalyst, also features low polarization resistances, high catalytic activity and stability, with retention of 81% of the catalyst layer capacitance after an initial 10 h longevity test, and delivery of a peak power of 1.14 W cm^{-2}. This is one of the highest power densities reported for an AEMFC containing a CRM-free cathode. This work shows the potential of the new field of HT-AEMFCs, opening opportunities for developing and using novel CRM-free catalysts that are highly active at these high operating temperatures.

1. Introduction

In recent years, awareness of the field of anion-exchange membrane fuel cells (AEMFCs) has increased significantly owing to the various benefits offered by the technology [1–3]. One of the features of using an alkali environment is the capacity to utilize a variety of platinum-group-metal-(PGM)-free electrocatalysts for the oxygen reduction reaction (ORR), which has resulted in an increasing number of technological advancements [4–15]. Whilst progress has been significant, it is worth noting that the majority of the recent reports involved catalysts containing critical raw materials (CRMs), such as platinum, palladium, and cobalt [16,17], with limited reports of AEMFCs containing CRM-free cathodes (Fig. S1 and Table S1). Additionally, most prior AEMFC reports used conventionally low testing temperatures (40 – 80 °C), including all PGM-free and CRM-free studies. In a recent review of AEMFCs, we [18] highlighted that most cell performance and longevity results were performed at an average of 60 °C, a temperature where many materials have high stability. Moreover, the majority of H_2-AEMFC performance results in the literature were still based on Pt catalysts. Currently, there are no reports of PGM-free or CRM-free cathode H_2-AEMFCs operating above 100 °C.

Yet, operating AEMFCs at such high temperatures has benefits: a simpler cell water management system; faster electrochemical reaction kinetics; reducing the overpotential losses during operation; decreasing the catalysts' sensitivity to fuel impurities; and improving stack cooling (on account of the thermal differential between the high operating temperature and ambient environment). All these would help realize deployment of more economical CRM-free catalysts in such fuel cells.

The plausibility of high-temperature AEMFCs (HT-AEMFCs) operation was successfully demonstrated in our previous work [19]. Using a thermally stable, radiation-grafted low-density polyethylene-(LDPE)-based anion-exchange membrane (AEM), we reported a hydroxide conductivity at 110 °C approaching 300 mS cm^{-1}. A Pt-based HT-AEMFC operated at 110 °C showed a remarkable reduction in performance losses in the mass transport (higher current density) region. Compared to conventional 60 – 80 °C operation with this AEM, a superior limiting current density of > 6 A cm^{-2} was achieved alongside a surprisingly reasonable peak power density (P_{max}) of 2.1 W cm^{-2} and 50 h voltage stability (at constant current density of 200 mA cm^{-2}).

We report here for the first time a CRM-free cathode HT-AEMFC

* Corresponding author.
E-mail address: dario@technion.ac.il (D.R. Dekel).

https://doi.org/10.1016/j.ceja.2021.100153
Received 3 March 2021; Received in revised form 25 June 2021; Accepted 8 July 2021
Available online 13 July 2021

operated at > 100 °C. The HT-AEMFC demonstrates excellent polarization performance, low in-situ cell resistance (ohmic and catalytic) and 81% retention of the cathode catalyst capacitance after 10 h of operation at this high-temperature.

2. Experimental

2.1. Anion conductivity and activation energy at high temperature

A previously established protocol reported by Ziv and Dekel [20] was used to measure the true hydroxide conductivity of a radiation-grafted ETFE-based benzyltrimethylammonium-(BTMA)-type AEM (IEC = 2.22 mmol g^{-1}, 55 ± 5 μm hydrated thickness) [21]. Briefly, the AEM was synthesized by exposing commercial 25 μm thick ETFE film (Nowofol) to 30 kGy absorbed radiation dose, followed by grafting with an aqueous dispersion (5 vol. %) of vinylbenzyl chloride monomer (Sigma-Aldrich, mixture of *meta*- and *para*-isomers) and a final amination step with aqueous 45 wt. % trimethylamine solution (Sigma-Aldrich) to form the radiation grafted AEM (designated henceforth as ETFE-BTMA-AEM). After establishing a stable true hydroxide conductivity at 60°C, 90% relative humidity (RH), and 0.85 barg back-pressure, the temperature was increased to 80 and then 105°C. The activation energy (E_a) was estimated via temperature-dependent conductivity, which follows the Arrhenius behavior expressed by Eq. (1):

$$\sigma = \sigma_0 \exp\left(-\frac{E_a}{k_B T}\right) \quad (1)$$

where σ_o is the pre-exponential factor (mS cm^{-1}), T the absolute temperature (K), E_a the activation energy (kJ mol^{-1}), and k_B is Boltzmann's constant (kJ K^{-1}).

2.2. Membrane electrode assembly fabrication

Gas diffusion electrodes (GDEs) were prepared by adapting our published method [19]. Briefly, the anode was made with PtRu/C, while the cathode contained 35 mg of N-doped-C (Fig. S2); both contained 15 mg of Fumion® polyaromate anion exchange ionomer functionalized with quaternary ammonium groups (IEC = 2.0 meq g^{-1}). The mixture was ground in one-part ultra-pure water and nine-parts of isopropyl alcohol to create the catalyst ink. 5 cm^2 active area anode and cathode GDEs were loaded to 0.7 mg_{PtRu} cm^{-2} and 1.11 $mg_{N\text{-}doped\text{-}C}$ cm^{-2}, respectively. Their optimal loadings with respect to CRM content are summarized in Table S2 (see supplementary material for details).

Both GDEs along with a 9 cm^2 piece of a ETFE-BTMA-based-AEM were immersed in petri dishes filled with aqueous 1 M KOH solution for 1 h, with solution changes every 20 min. They were then assembled into an AEMFC between two 5 cm^2 single-serpentine graphite bipolar flow field plates with a torque of 4.5 N m.

2.3. Anion-exchange membrane fuel cell electrochemical testing

The AEMFC start-up testing protocol used was similar to that previously reported [19], where a stable, maximum current density of 1.5 A cm^{-2} was obtained at 60 °C before testing. An initial polarization curve was then recorded at a scan rate of 5 mV s^{-1} to quickly capture beginning-of-life performance. Following this, the current was set to 3 A and the corresponding voltage was allowed to stabilize for ~3 min. Then an electrochemical impedance spectrum (EIS) was recorded (*f* scan 10, 000 → 0.1 Hz with 20 steps dec^{-1} and an AC amplitude perturbation of 5% of the current). The polarization curve and cell impedance scans were repeated in a similar manner after the cell temperature was increased to 80 °C (optimized dewpoints and a back-pressure of 1 barg). Finally, the cell temperature was increased to 105 °C (further optimized dewpoints and a back-pressure of 1.4 barg). After these tests, the cathode gas was switched from O_2 to N_2 (15 min flow at the open circuit voltage (OCV)) to purge all traces of O_2. An initial cyclic voltammogram (CV) was then recorded (between 0.05 and 1 V at 100 mV sec^{-1}). The cathode gas was then reverted to O_2 (until a stable high OCV was attained) before discharging the cell at a current density of 500 mA cm^{-2} for 10 h. Finally, following this voltage stability test, a second CV (after N_2 purge) was recorded from the cathode, where the initial and final capacitances were compared using Eq. (2) [22]:

$$C = \frac{\int IdV}{2mvdV} \quad (2)$$

where C is the capacitance (F g^{-1}), dV is the potential range (V), IdV is the area under the cyclic voltammogram, m is the mass (g), and ν is the scan rate (V s^{-1}).

3. Results and Discussion

We have measured the performance of the ETFE-BTMA-based AEM at temperatures below and above 100 °C after which we evaluated the performance of *in operando* AEMFC with a CRM-free N-doped-C cathode at the same temperatures.

3.1. High-temperature hydroxide conductivity and activation energy

Fig. 1(a) shows the anion conductivity of the AEM during decarbonation. Following 1 h of stabilization at 60 °C (AEM started off in its bicarbonate form), a direct current of 0.1 mA was applied, causing OH^-

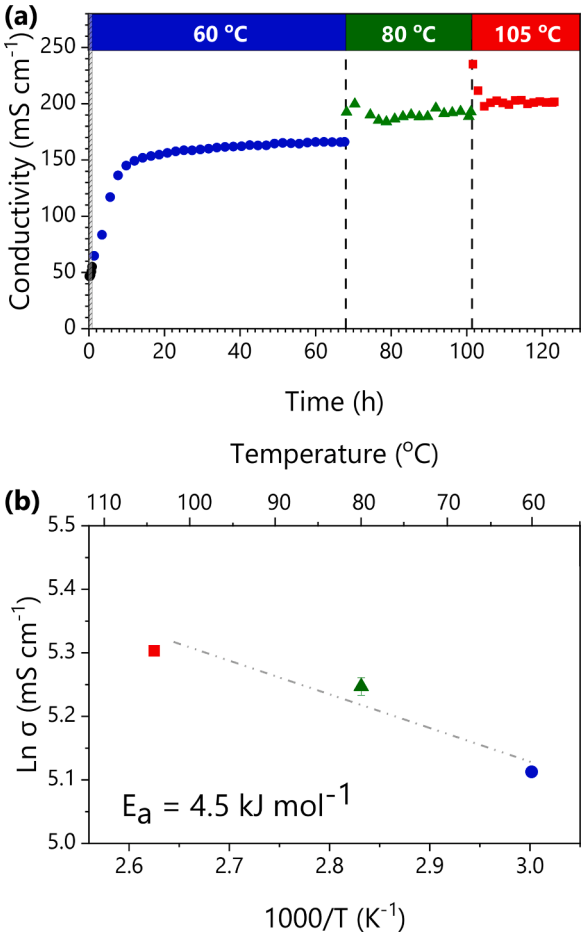

Figure 1. (a) "True" OH^- conductivity (4-probe) of the radiation-grafted ETFE-BTMA-based AEM, measured at 60, 80, and 105°C. Conditions: 0.1 mA direct current, N_2 flow of 500 mL min^{-1} at 90% RH. (b) Arrhenius plots using the data extracted from (a).

generation via water electrolysis and HCO_3^- to be purged from the AEM via CO_2 evolution. During the exchange of the HCO_3^- to OH^- (Fig. 1a blue), the conductivity rapidly increases (OH^- ions have higher mobility). After 30 – 40 h, the AEM is in its true OH^- form, yielding a stable conductivity plateau known as the true OH^- conductivity (166 mS cm^{-1}, *cf.* 152 mS cm^{-1} reported by Zhegur-Khais *et al.* [23]). Transient sharp increases in the conductivities are initially seen as the temperature is raised first to 80 °C and then to 105 °C due to temperature and humidity fluctuations after the changes. The AEM's true OH^- conductivity increases with temperature (as expected [24–30]): values of 190 and 201 mS cm^{-1} were obtained at 80 °C (Fig. 1a green) and 105 °C (Fig. 1a red), respectively. Due to the high testing temperature, the true OH^- conductivity measured is among the highest values reported for AEMs.

The activation energy (E_a) of 4.5 kJ mol^{-1} (0.045 eV), calculated from the true OH^- conductivities of the AEM (Fig. 1b), is among the lowest reported for AEMs (Table S3) and is even lower than that of the Nafion® H^+-conducting membrane [31,32]. For example, Paul *et al.* [31] measured E_a values ranging between 9 and 15 kJ mol^{-1}, while Matos et al. [32] obtained 5.9 – 10.6 kJ mol^{-1}. A low E_a value is preferable, as it indicates a lower barrier for the OH^- conduction. Additionally, the higher mobility of the OH^- ions and the increased hydration levels at the high temperature (formation of continuous hydrated ion-conducting channels through the AEM [33,34]) further contribute to the low E_a values, all of which is consistent with OH^- transport occuring via a Grotthuss-type mechanism [35,36].

3.2. High-temperature AEMFC electrochemical tests

The ORR and HOR performances at 60, 80, and 105 °C for the AEMFC containing the CRM-free N-doped-C cathode are presented in Fig. 2. Similar to our previous study that used Pt-based cathodes [19], operating above 100 °C led to significant improvements. The limiting current density increased from ~2.2 A cm^{-2} at 80 °C to ~3.0 A cm^{-2} at 105 °C (Fig. 2a). We hypothesize that this relates to enhanced catalytic activity in the kinetic region (see inset in Fig. 2a, Table S4 gives a detailed comparison of cell performance in the kinetic region of each IV curve). The current density at 0.65 V increases from 0.85 to 1.17 A cm^{-2} from 80 to 105 °C, respectively. This enhancement extends into the ohmic region, where the high temperatures lead to higher OH^- conductivity (Fig. 1).

These results are the first reported HT-AEMFC with a CRM-free cathode. To the best of our knowledge, peak power density P_{max} = 1.14 W cm^{-2} (Fig. 2b), limiting current density = 2.93 A cm^{-2}, and current density = 2.28 A cm^{-2} at 0.6 V, all outperform recently reported data collected with AEMFCs containing CRM-free cathodes (Table S1 and Fig. S3, admittedly at lower test temperatures). For instance, Lu *et al.* [15] reported a P_{max} and current density values at Lus 60 °C of 0.70 W cm^{-2} and 1.0 A cm^{-2} at 0.60 V, respectively, using a Halloysite-derived furfural urea N-doped-C cathode (1.0 $mg_{catalyst}$ cm^{-2}). In another report by Pham *et al.* [37] using a F-, N-, and S-tri-doped reduced graphene oxide cathode (1.5 $mg_{catalyst}$ cm^{-2}), P_{max} and current density values at 85 °C of 0.05 W cm^{-2} and 0.02 A cm^{-2}, respectively, were obtained at 0.60 V. When comparing with a wider range of reports of AEMFCs containing PGM-free cathodes, this CRM-free cathode cell is among the highest in terms of P_{max}, with the highest current density at 0.6 V (Table S5).

The performance of this first-reported CRM-free-cathode HT-AEMFC in the kinetic (low current density) region is already comparable to the state-of-the-art proton exchange membrane fuel cells (PEMFCs) and superior to literature reported HT-PEMFCs with PGM-free cathodes under H_2/O_2 gas flows [38–41]. As found in the recent PEMFC literature, Fu *et al.* [41] employed a 3D-porous Fe-N-C catalyst tested at 80 °C yielding a P_{max} of 1.06 W cm^{-2}, a limiting current density of 3.4 A cm^{-2}, and a current density of 1.5 A cm^{-2} at 0.60 V. In the HT-PEMFC literature, current densities at 0.6 V are < 0.25 A cm^{-2} for cells operated at 120–180 °C [42–47], compared to 2.28 A cm^{-2} for our HT-AEMFC at 105 °C.

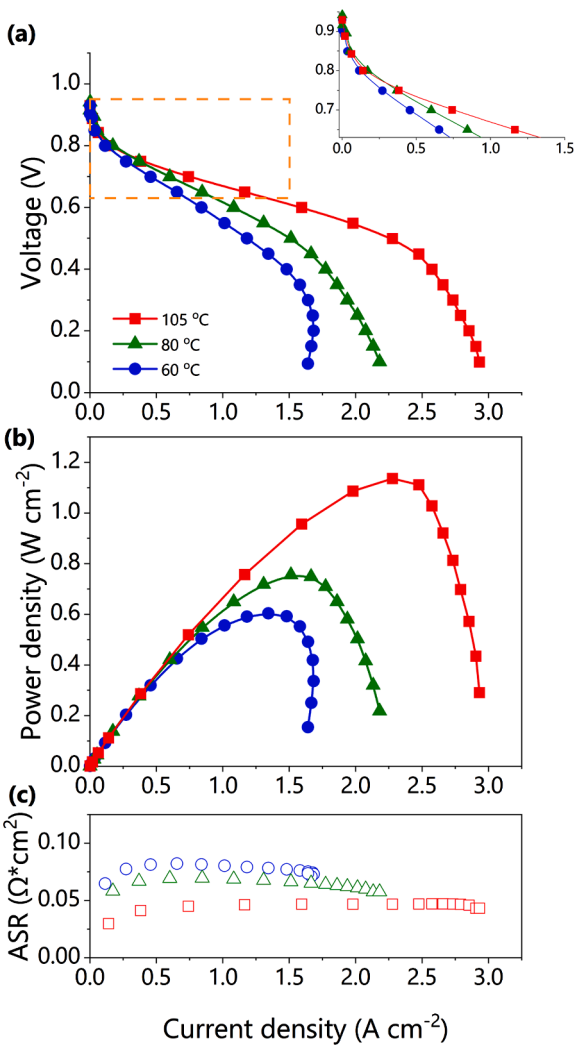

Figure 2. AEMFC test data with H_2/O_2 gas flows of 1 L min^{-1} under the following conditions: cell temperature of 105 °C with optimized dewpoints and 1.4 barg back-pressurization on both electrodes; 80 °C with optimized dewpoints and 1 barg back-pressurization on both electrodes; and 60 °C with optimized dewpoints and no back-pressurization. (a) Voltage-current density curves (inset shows a zoom-in of the dashed area), (b) Power density-current density curves, and (c) ASR-current density curves. All data was collected at 5 mV s^{-1}. See Table S6 for optimized dewpoint temperature information.

We also observed a lower mean area-specific resistance (ASR) of 0.04 Ω cm^2 during the acquisition of the polarization curve (Fig. 2c). These combined improvements gave a 50% increase in P_{max} from 0.76 W cm^{-2} → 1.14 W cm^{-2} when moving from 80 °C → 105 °C.

Fig. 3a shows the results of the EIS measurements performed in H_2/O_2 flow conditions under a current load of 600 mA cm^{-2}. When increasing the operating temperature from 60 to 105 °C, the semicircles' low-frequency resistance limit decreased gradually from 0.05 to 0.028 Ω cm^2, attributed to the improved catalytic processes. This trend is congruent with the understanding that as the kinetic energy of the reactants increases due to temperature, they overcome the activation energy barrier more easily thereby improving the rate of reaction [48,49]. Improved catalytic performances of both the hydrogen oxidation and oxygen reduction reactions are known to increase with increasing temperature [50–52]. A corresponding decrease in the high-frequency resistance from 0.017 to 0.01 Ω cm^2 is due to the increased OH^- conductivity through the AEM (as discussed above) coupled with the overall lower ohmic resistance of the cell. The EIS data are in line with the

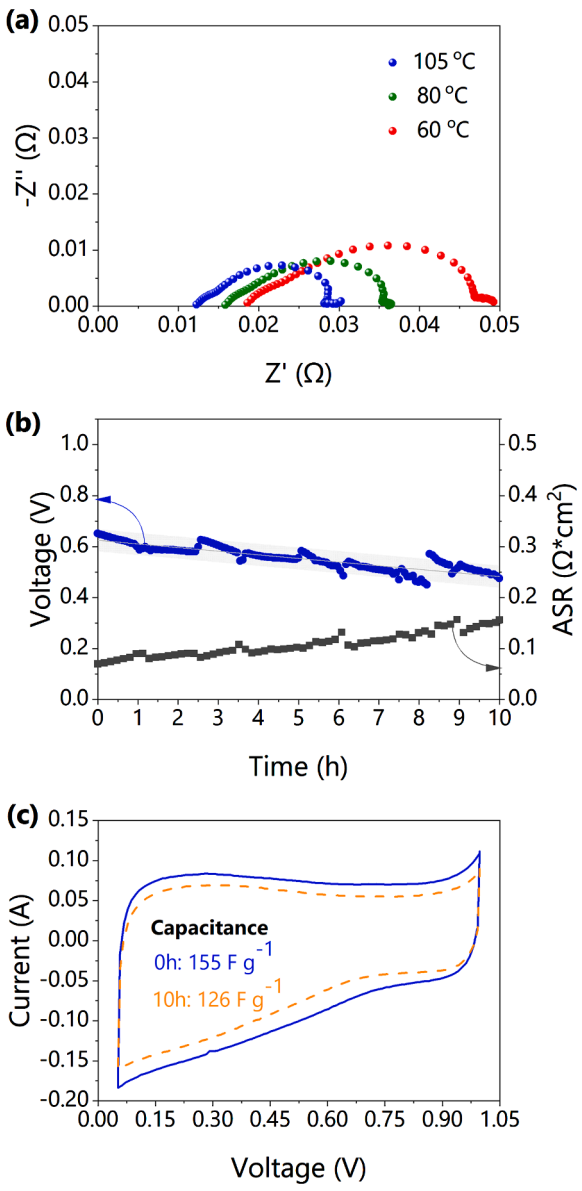

Figure 3. (a) H_2/O_2 in-situ EIS data collected at 60, 80, and 105 °C (10,000 → 0.1 Hz AC amplitude = 5% of the current); (b) An initial 10 h operando durability test at a cell temperature of 105 °C with a constant current density discharge of 500 mA cm^{-2}; (c) In-situ H_2/N_2 CV data for the N-doped-C both before and after the 10 h stability test (100 mV s^{-1}).

improved cell performance, further reflecting both the improved conductivity and reaction kinetics at higher temperature. These in-situ resistances are about four times lower than those reported for AEMFCs operated at 60 °C with high-performance PGM-free cathodes [53–55].

We also ran an initial 10 h high-temperature stability test at a constant current density discharge of 500 mA cm^{-2} (Fig. 3b), observing a voltage degradation of 14 mV h^{-1}. This stability will undoubtedly improve with optimized materials and HT-AEMFC operating parameters. To further probe degradation, we performed in-situ CV tests of the N-doped-C cathode both before and after this 10 h constant current density test to evaluate any capacitance changes. As shown in Fig. 3c, 81% retention of the total capacitance was achieved, suggesting that the cathode catalyst is relatively stable, and that the decrease in the cell performance cannot solely be attributed to the catalyst. AEM and iomomer degradation would also play a role in the performance loss at these temperatures and this needs to be decoupled in a future study.

4. Conclusion

We have built upon our first work on a HT-AEMFCs (with PGM catalysts) by incorporating a highly active CRM-free cathode. At 105 °C, the AEM showed a true OH^- conductivity of 201 mS cm^{-1}. The HT-AEMFC containing a N-doped-C (CRM-free) cathode delivered a peak power density of 1.14 W cm^{-2} and reached a limiting current desity of 2.9 A cm^{-2}, with realization of a reduced cell resistance at 105 °C. Furthermore, this first PGM-free-cathode HT-AEMFC outperformed all recently reported HT-PEMFCs, which were tested at even higher temperatures. This work demonstrates the potential of operating AEMFCs with PGM-free, and even CRM-free, cathodes at high temperatures. Additionally, it incentivizes the advancement of CRM-free catalysts, which reduces manufacturing supply chain risks with such strategic renewable energy technologies.

Declaration of Competing Interest

The authors declare that they have no known competing financial interests or personal relationships that could have appeared to influence the work reported in this paper.

Acknowledgements

This work was partially funded by the Nancy & Stephen Grand Technion Energy Program (GTEP); the Ministry of National Infrastructure, Energy and Water Resources of Israel through grants and No. 3-16686 (219-11-135), and the Planning & Budgeting Committee / ISRAEL Council for Higher Education (CHE) and Fuel Choice Initiative (Prime Minister Office of ISRAEL), within the framework of "Israel National Research Center for Electrochemical Propulsion (INREP)". The AEMs were fabricated using funds from EPSRC (UK) grant EP/R044163/1. We thank L. Jiang (Technion) for assisting with the AEMFC anode preparation. J.B., G.R. and N.Y. acknowledge financial support from the Netherlands Organization for Scientific Research (NWO) NWO-GDST Advanced Materials program (729.001.022).

Supplementary materials

Supplementary material associated with this article can be found, in the online version, at doi:10.1016/j.ceja.2021.100153.

References

[1] D.R. Dekel, I. Rasin, M. Page, S. Brandon, Steady state and transient simulation of anion exchange membrane fuel cells, J. Power Sources. 375 (2018) 191–204, https://doi.org/10.1016/j.jpowsour.2017.07.012.
[2] C.G. Arges, L. Zhang, Anion Exchange Membranes' Evolution toward High Hydroxide Ion Conductivity and Alkaline Resiliency, ACS Appl. Energy Mater. 1 (2018) 2991–3012, https://doi.org/10.1021/acsaem.8b00387.
[3] H. Shiau, I. V Zenyuk, A.Z. Weber, Elucidating Performance Limitations in Alkaline-Exchange- Membrane Fuel Cells, 164 (2017). https://doi.org/10.1149/2.0531711jes.
[4] I. Kruusenberg, D. Ramani, S. Ratso, U. Joost, R. Saar, P. Rauwel, A.M. Kannan, K. Tammeveski, Cobalt–Nitrogen Co-doped Carbon Nanotube Cathode Catalyst for Alkaline Membrane Fuel Cells, ChemElectroChem 3 (2016) 1455–1465, https://doi.org/10.1002/celc.201600241.
[5] V.M. Truong, J.R. Tolchard, J. Svendby, M. Manikandan, H.A. Miller, S. Sunde, H. Yang, D.R. Dekel, A.O. Barnett, Platinum and platinum group metal-free catalysts for anion exchange membrane fuel cells, Energies 13 (2020) 1–21, https://doi.org/10.3390/en13030582.
[6] Y.J. Sa, D.J. Seo, J. Woo, J.T. Lim, J.Y. Cheon, S.Y. Yang, J.M. Lee, D. Kang, T. J. Shin, H.S. Shin, H.Y. Jeong, C.S. Kim, M.G. Kim, T.Y. Kim, S.H. Joo, A General Approach to Preferential Formation of Active Fe-Nx Sites in Fe-N/C Electrocatalysts for Efficient Oxygen Reduction Reaction, J. Am. Chem. Soc. 138 (2016) 15046–15056, https://doi.org/10.1021/jacs.6b09470.
[7] H. Ren, Y. Wang, Y. Yang, X. Tang, Y. Peng, H. Peng, L. Xiao, J. Lu, H.D. Abruña, L. Zhuang, Fe/N/C nanotubes with atomic Fe sites: A highly active cathode catalyst for alkaline polymer electrolyte fuel cells, ACS Catal 7 (2017) 6485–6492, https://doi.org/10.1021/acscatal.7b02340.
[8] R. Sibul, E. Kibena-Põldsepp, S. Ratso, M. Kook, M.T. Sougrati, M. Käärik, M. Merisalu, J. Aruväli, P. Paiste, A. Treshchalov, J. Leis, V. Kisand, V. Sammelselg,

S. Holdcroft, F. Jaouen, K. Tammeveski, Iron- and Nitrogen-Doped Graphene-Based Catalysts for Fuel Cell Applications, ChemElectroChem 7 (2020) 1739–1747, https://doi.org/10.1002/celc.202000011.
[9] A. Sarapuu, E. Kibena-Põldsepp, M. Borghei, K. Tammeveski, Electrocatalysis of oxygen reduction on heteroatom-doped nanocarbons and transition metal-nitrogen-carbon catalysts for alkaline membrane fuel cells, J. Mater. Chem. A. 6 (2018) 776–804, https://doi.org/10.1039/c7ta08690c.
[10] J. Lilloja, E. Kibena-Põldsepp, A. Sarapuu, J.C. Douglin, M. Käärik, J. Kozlova, P. Paiste, A. Kikas, J. Aruväli, J. Leis, V. Sammelselg, D.R. Dekel, K. Tammeveski, Transition-Metal- and Nitrogen-Doped Carbide-Derived Carbon/Carbon Nanotube Composites as Cathode Catalysts for Anion-Exchange Membrane Fuel Cells, ACS Catal (2021) 1920–1931, https://doi.org/10.1021/acscatal.0c03511.
[11] J. Biemolt, J.C. Douglin, R.K. Singh, E.S. Davydova, N. Yan, G. Rothenberg, D. R. Dekel, An Anion - Exchange Membrane Fuel Cell Containing Only Abundant and Affordable Materials, Energy Technol (2021), 202000909, https://doi.org/10.1002/ente.202000909.
[12] R. Praats, M. Käärik, A. Kikas, V. Kisand, J. Aruväli, P. Paiste, M. Merisalu, A. Sarapuu, J. Leis, V. Sammelselg, J.C. Douglin, D.R. Dekel, K. Tammeveski, Electroreduction of oxygen on cobalt phthalocyanine-modified carbide-derived carbon/carbon nanotube composite catalysts, J. Solid State Electrochem. 25 (2021) 57–71, https://doi.org/10.1007/s10008-020-04543-z.
[13] H.A. Firouzjaie, W.E. Mustain, Catalytic Advantages, Challenges, and Priorities in Alkaline Membrane Fuel Cells, ACS Catal 10 (2020) 225–234, https://doi.org/10.1021/acscatal.9b03892.
[14] X. Peng, T.J. Omasta, E. Magliocca, L. Wang, J.R. Varcoe, W.E. Mustain, Nitrogen-doped Carbon–CoO x Nanohybrids: A Precious Metal Free Cathode that Exceeds 1.0 W cm −2 Peak Power and 100 h Life in Anion-Exchange Membrane Fuel Cells, Angew. Chem. Int. Ed. 58 (2019) 1046–1051, https://doi.org/10.1002/anie.201811099.
[15] Y. Lu, L. Wang, K. Preuß, M. Qiao, M.M. Titirici, J. Varcoe, Q. Cai, Halloysite-derived nitrogen doped carbon electrocatalysts for anion exchange membrane fuel cells, J. Power Sources. 372 (2017) 82–90, https://doi.org/10.1016/j.jpowsour.2017.10.037.
[16] Critical Raw Materials for Strategic Technologies and Sectors in the EU, 2020. https://doi.org/10.2873/58081.
[17] J. Santillán-Saldivar, A. Cimprich, N. Shaikh, B. Laratte, S.B. Young, G. Sonnemann, How recycling mitigates supply risks of critical raw materials: Extension of the geopolitical supply risk methodology applied to information and communication technologies in the European Union, Resour. Conserv. Recycl. 164 (2021), 105108, https://doi.org/10.1016/j.resconrec.2020.105108.
[18] D.R. Dekel, Review of cell performance in anion exchange membrane fuel cells, J. Power Sources. 375 (2018) 158–169, https://doi.org/10.1016/j.jpowsour.2017.07.117.
[19] J.C. Douglin, J.R. Varcoe, D.R. Dekel, A high-temperature anion-exchange membrane fuel cell, J. Power Sources Adv. 5 (2020), 100023, https://doi.org/10.1016/j.powera.2020.100023.
[20] N. Ziv, D.R. Dekel, A practical method for measuring the true hydroxide conductivity of anion exchange membranes, Electrochem. Commun. 88 (2018) 109–113, https://doi.org/10.1016/j.elecom.2018.01.021.
[21] L. Wang, E. Magliocca, E.L. Cunningham, W.E. Mustain, S.D. Poynton, R. Escudero-Cid, M.M. Nasef, J. Ponce-González, R. Bance-Souahli, R.C.T. Slade, D. K. Whelligan, J.R. Varcoe, An optimised synthesis of high performance radiation-grafted anion-exchange membranes, Green Chem 19 (2017) 831–843, https://doi.org/10.1039/C6GC02526A.
[22] T. Kar, R. Devivaraprasad, R.K. Singh, B. Bera, M. Neergat, Reduction of graphene oxide – a comprehensive electrochemical investigation in alkaline and acidic electrolytes, RSC Adv 4 (2014) 57781–57790, https://doi.org/10.1039/C4RA10794B.
[23] A. Zhegur-Khais, F. Kubannek, U. Krewer, D.R. Dekel, Measuring the true hydroxide conductivity of anion exchange membranes, J. Memb. Sci. 612 (2020), 118461, https://doi.org/10.1016/j.memsci.2020.118461.
[24] L. Wang, M. Bellini, H.A. Miller, J.R. Varcoe, A high conductivity ultrathin anion-exchange membrane with 500+ h alkali stability for use in alkaline membrane fuel cells that can achieve 2 W cm^{-2} at 80°C, J. Mater. Chem. A. 6 (2018) 15404–15412, https://doi.org/10.1039/c8ta04783a.
[25] H.S. Dang, P. Jannasch, High-Performing Hydroxide Exchange Membranes with Flexible Tetra-Piperidinium Side Chains Linked by Alkyl Spacers, ACS Appl. Energy Mater. 1 (2018) 2222–2231, https://doi.org/10.1021/acsaem.8b00294.
[26] A. Zhegur, N. Gjineci, S. Willdorf-Cohen, A.N. Mondal, C.E. Diesendruck, N. Gavish, D.R. Dekel, Changes of Anion Exchange Membrane Properties During Chemical Degradation, ACS Appl. Polym. Mater. 2 (2020) 360–367, https://doi.org/10.1021/acsapm.9b00838.
[27] M. Mandal, G. Huang, P.A. Kohl, Highly Conductive Anion-Exchange Membranes Based on Cross-Linked Poly(norbornene): Vinyl Addition Polymerization, ACS Appl. Energy Mater. 2 (2019) 2447–2457, https://doi.org/10.1021/acsaem.8b02051.
[28] J. Müller, A. Zhegur, U. Krewer, J.R. Varcoe, D.R. Dekel, Practical ex-Situ Technique to Measure the Chemical Stability of Anion-Exchange Membranes under Conditions Simulating the Fuel Cell Environment, ACS Mater. Lett. 2 (2020) 168–173, https://doi.org/10.1021/acsmaterialslett.9b00418.
[29] Z. Li, X. He, Z. Jiang, Y. Yin, B. Zhang, G. He, Z. Tong, H. Wu, K. Jiao, Enhancing Hydroxide Conductivity and Stability of Anion Exchange Membrane by Blending Quaternary Ammonium Functionalized Polymers, Electrochim. Acta. 240 (2017) 486–494, https://doi.org/10.1016/j.electacta.2017.04.109.
[30] N. Li, M.D. Guiver, W.H. Binder, Towards High Conductivity in Anion-Exchange Membranes for Alkaline Fuel Cells, ChemSusChem 6 (2013) 1376–1383, https://doi.org/10.1002/cssc.201300320.
[31] D.K. Paul, R. McCreery, K. Karan, Proton Transport Property in Supported Nafion Nanothin Films by Electrochemical Impedance Spectroscopy, J. Electrochem. Soc. 161 (2014) F1395–F1402, https://doi.org/10.1149/2.0571414jes.
[32] B.R. Matos, C.A. Goulart, E.I. Santiago, R. Muccillo, F.C. Fonseca, Proton conductivity of perfluorosulfonate ionomers at high temperature and high relative humidity, Appl. Phys. Lett. 104 (2014), https://doi.org/10.1063/1.4867351.
[33] C. Wang, B. Mo, Z. He, X. Xie, C.X. Zhao, L. Zhang, Q. Shao, X. Guo, E.K. Wujcik, Z. Guo, Hydroxide ions transportation in polynorbornene anion exchange membrane, Polymer (Guildf) 138 (2018) 363–368, https://doi.org/10.1016/j.polymer.2018.01.079.
[34] T. Zelovich, M.E. Tuckerman, Water Layering Affects Hydroxide Diffusion in Functionalized Nanoconfined Environments, J. Phys. Chem. Lett. 11 (2020) 5087–5091, https://doi.org/10.1021/acs.jpclett.0c01141.
[35] X. Gao, F. Lu, B. Dong, A. Wu, N. Sun, L. Zheng, Anion exchange membranes with well-defined ion transporting nanochannels: Via self-assembly of polymerizable ionic liquids, J. Mater. Chem. A. 4 (2016) 13316–13326, https://doi.org/10.1039/c6ta05223a.
[36] V. Dubey, A. Maiti, S. Daschakraborty, Predicting the solvation structure and vehicular diffusion of hydroxide ion in an anion exchange membrane using nonreactive molecular dynamics simulation, Chem. Phys. Lett. 755 (2020), 137802, https://doi.org/10.1016/j.cplett.2020.137802.
[37] C. Van Pham, M. Klingele, B. Britton, K.R. Vuyyuru, T. Unmuessig, S. Holdcroft, A. Fischer, S. Thiele, Tridoped Reduced Graphene Oxide as a Metal-Free Catalyst for Oxygen Reduction Reaction Demonstrated in Acidic and Alkaline Polymer Electrolyte Fuel Cells, Adv. Sustain. Syst. 1 (2017), 1600038, https://doi.org/10.1002/adsu.201600038.
[38] Y. Nabae, S. Nagata, T. Hayakawa, H. Niwa, Y. Harada, M. Oshima, A. Isoda, A. Matsunaga, K. Tanaka, T. Aoki, Pt-free carbon-based fuel cell catalyst prepared from spherical polyimide for enhanced oxygen diffusion, Sci. Rep. 6 (2016) 1–7, https://doi.org/10.1038/srep23276.
[39] H.T. Chung, D.A. Cullen, D. Higgins, B.T. Sneed, E.F. Holby, K.L. More, P. Zelenay, Direct atomic-level insight into the active sites of a high-performance PGM-free ORR catalyst, Science 357 (2017) 479–484, https://doi.org/10.1126/science.aan2255.
[40] L. Osmieri, J. Park, D.A. Cullen, P. Zelenay, D.J. Myers, K.C. Neyerlin, Status and challenges for the application of platinum group metal-free catalysts in proton-exchange membrane fuel cells, Curr. Opin. Electrochem. 25 (2021), 100627, https://doi.org/10.1016/j.coelec.2020.08.009.
[41] X. Fu, P. Zamani, J.Y. Choi, F.M. Hassan, G. Jiang, D.C. Higgins, Y. Zhang, M. A. Hoque, Z. Chen, Situ Polymer Graphenization Ingrained with Nanoporosity in a Nitrogenous Electrocatalyst Boosting the Performance of Polymer-Electrolyte-Membrane Fuel Cells, Adv. Mater. 29 (2017), https://doi.org/10.1002/adma.201604456.
[42] D. Peterson, Innovative Non-PGM Catalysts for High-Temperature PEMFCs, n.d. https://www.hydrogen.energy.gov/pdfs/review17/fc132_mukerjee_2017_o.pdf.
[43] R. Gokhale, T. Asset, G. Qian, A. Serov, K. Artyushkova, B.C. Benicewicz, P. Atanassov, Implementing PGM-free electrocatalysts in high-temperature polymer electrolyte membrane fuel cells, Electrochem. Commun. 93 (2018) 91–94, https://doi.org/10.1016/j.elecom.2018.06.019.
[44] Y. Hu, J.O. Jensen, C. Pan, L.N. Cleemann, I. Shypunov, Q. Li, Immunity of the Fe-N-C catalysts to electrolyte adsorption: Phosphate but not perchloric anions, Appl. Catal. B Environ. 234 (2018) 357–364, https://doi.org/10.1016/j.apcatb.2018.03.056.
[45] W. Li, D. Wang, Y. Zhang, L. Tao, T. Wang, Y. Zou, Y. Wang, R. Chen, S. Wang, Defect Engineering for Fuel-Cell Electrocatalysts, Adv. Mater. 32 (2020) 1–20, https://doi.org/10.1002/adma.201907879.
[46] Y. Cheng, S. He, S. Lu, J.P. Veder, B. Johannessen, L. Thomsen, M. Saunders, T. Becker, R. De Marco, Q. Li, S. ze Yang, S.P. Jiang, Iron Single Atoms on Graphene as Nonprecious Metal Catalysts for High-Temperature Polymer Electrolyte Membrane Fuel Cells, Adv. Sci. 6 (2019), https://doi.org/10.1002/advs.201802066.
[47] R. Haider, Y. Wen, Z.-F. Ma, D.P. Wilkinson, L. Zhang, X. Yuan, S. Song, J. Zhang, High temperature proton exchange membrane fuel cells: progress in advanced materials and key technologies, Chem. Soc. Rev. (2021), https://doi.org/10.1039/d0cs00296h.
[48] R. O'hayre, S.-W. Cha, W. Colella, F.B. Prinz, Fuel cell fundamentals, John Wiley & Sons, 2016.
[49] T.S. Zhao, Anion Exchange Membrane Fuel Cells, Springer International Publishing, Cham, Switzerland, 2018.
[50] Q. Li, H. Peng, Y. Wang, L. Xiao, J. Lu, L. Zhuang, The Comparability of Pt to Pt-Ru in Catalyzing the Hydrogen Oxidation Reaction for Alkaline Polymer Electrolyte Fuel Cells Operated at 80°C, Angew. Chemie - Int, Ed. 58 (2019) 1442–1446, https://doi.org/10.1002/anie.201812662.
[51] B. Lim, M. Jiang, P.H.C. Camargo, E.C. Cho, J. Tao, X. Lu, Y. Zhu, Y. Xia, Pd-Pt bimetallic nanodendrites with high activity for oxygen reduction, Science 324 (80) (2009) 1302–1305, https://doi.org/10.1126/science.1170377.
[52] F. Yang, X. Bao, Y. Zhao, X. Wang, G. Cheng, W. Luo, Enhanced HOR catalytic activity of PGM-free catalysts in alkaline media: the electronic effect induced by different heteroatom doped carbon supports, J. Mater. Chem. A. 7 (2019) 10936–10941, https://doi.org/10.1039/C9TA01916B.
[53] J. Lilloja, E. Kibena-Põldsepp, A. Sarapuu, A. Kikas, V. Kisand, M. Käärik, M. Merisalu, A. Treshchalov, J. Leis, V. Sammelselg, Q. Wei, S. Holdcroft, K. Tammeveski, Nitrogen-doped carbide-derived carbon/carbon nanotube

composites as cathode catalysts for anion exchange membrane fuel cell application, Appl. Catal. B Environ. 272 (2020), 119012, https://doi.org/10.1016/j.apcatb.2020.119012.

[54] G.A. Goenaga, A.L. Roy, N.M. Cantillo, S. Foister, T.A. Zawodzinski, A family of platinum group metal-free catalysts for oxygen reduction in alkaline media, J. Power Sources. 395 (2018) 148–157, https://doi.org/10.1016/j.jpowsour.2018.05.025.

[55] H.A. Miller, M.V Pagliaro, M. Bellini, F. Bartoli, L. Wang, I. Salam, J.R. Varcoe, F. Vizza, Integration of a Pd-CeO2/C Anode with Pt and Pt-Free Cathode Catalysts in High Power Density Anion Exchange Membrane Fuel Cells, ACS Appl. Energy Mater. 3 (2020) 10209–10214, https://doi.org/10.1021/acsaem.0c01998.